Biological and environmental rhythms in (dark) deep-sea hydrothermal ecosystems

Daphne Cuvelier[1,2]*, Pierre Legendre[3], Agathe Laes-Huon[4], Pierre-Marie Sarradin[1], Jozée Sarrazin[1]

[1.] Ifremer, Centre de Bretagne, REM/EEP, Laboratoire Environnement Profond, Plouzané, 29280, France
[2.] Mare - Marine and Environmental Sciences Centre, Department of Oceanography and Fisheries, Rua Professor Frederico Machado 4, Horta, 9901-862, Portugal §
[3.] Département de Sciences Biologiques, Université de Montréal, C.P. 6128, succursale Centre-ville, Montréal, H3C 3J7, Québec, Canada
[4.] Ifremer, Centre de Bretagne, REM/RDT, Laboratoire Détection, Capteurs et Mesures, Plouzané, 29280, France

*correspondence to: Daphne Cuvelier (daphne.cuvelier@gmail.com)
§ Current address of corresponding author

Abstract

During 2011, two deep-sea observatories focusing on hydrothermal vent ecology were up and running in the Atlantic (Eiffel Tower, Lucky Strike vent field) and the North-East Pacific Ocean (NEP) (Grotto, Main Endeavour field). Both ecological modules recorded imagery and environmental variables jointly for a time span of 23 days (7-30 October 2011) and environmental variables for up to 9 months (October 2011 to June 2012). Community dynamics were assessed based on imagery analysis and rhythms in temporal variation for both fauna and environment were revealed. Tidal rhythms were found to be at play in the two settings and were most visible in temperature and tubeworm appearances (at NEP). A 6-hour lag in tidal rhythm occurrence was observed between Pacific and Atlantic hydrothermal vents which corresponds to the geographical distance and time delay between the two sites.

1. Introduction

All over our planet, animals are influenced by day- and night-cycles. Entrainment occurs when rhythmic physiological or behavioural events in animals match the periods and phase of an environmental oscillation, e.g. circadian rhythms to light-dark cycles. In marine populations such cycles are evident in the photic zone (Naylor 1985). However, more recently similar cycles have become apparent in deep-sea organisms and populations as well, at depths where light does not penetrate. At these greater depths, fluctuations in light intensity are likely to be replaced by changes in hydrodynamic conditions (Aguzzi et al., 2010). Several studies reveal the presence of tidal cycles in environmental variables (such as currents, fluid emission, temperature) in the deep sea, particularly at hydrothermal vents (e.g. Tivey et al., 2002; Thomsen et al., 2012; Barreyre et al., 2014; Sarrazin et al., 2014) and the influence of tides on the deep-sea organisms was already previously inferred. In meantime, an actual tidal rhythm has been revealed in visible faunal densities and appearance rate for inhabitants of various deep-sea chemosynthetic environments (e.g. a semi-diurnal tidal component in buccinids at cold seeps (Aguzzi et al., 2010) and semi-diurnal and diurnal tidal components in siboglinids (Tunnicliffe et al., 1990; Cuvelier et al., 2014)).

41   Presumably, though difficult to statistically demonstrate, the deep-sea organisms reflect or respond to the changing

42   surrounding environmental conditions, which are modulated by hydrodynamic processes including the tides.

43

44   Despite the growing realisation that tidal influences are indeed at play in the deep ocean, it remains hard to actually

45   reveal these patterns because of the isolation of the ecosystem and the limited access to the longer time-series. The

46   use of deep-sea observatories, which have been deployed recently in various seas and oceans (see Puillat et al.,

47   2012 for an overview) brings out new insights into the dynamics of these remote habitats. First ecological analyses

48   based on deep-sea observatories have been published (Juniper et al., 2013; Matabos et al., 2014; 2015; Cuvelier et

49   al., 2014; Sarrazin et al., 2014), and many more works are in progress.

50

51   The current observatory-based study allows a unique comparison of hydrothermal vent community dynamics

52   between two different oceans featuring a different seafloor spreading rate. Data originating from the deep-sea

53   observatories on the slow-spreading Mid-Atlantic Ridge (MoMAR, now EMSO-Açores) and on the faster-

54   spreading Juan de Fuca Ridge (North-East Pacific, NEPTUNE, now called Ocean Networks Canada (ONC)),

55   featuring the exact same time span and resolution, have been analysed. Whilst the two oceans are characterised by

56   different vent fauna, they do share higher taxonomic groups. Key questions put forward are: (i) Are tidal rhythms

57   discernible in both hydrothermal settings? (ii) Is there a lag/time difference in community dynamics and

58   environmental variables observed between the two oceans? (iii) Which environmental variables influence

59   community dynamics the most? and finally (iv) Do the shared taxa occupy similar microhabitats and possible

60   niches in each ocean? Answering these questions will provide new insights in understanding local vent community

61   dynamics and will enlighten us on similarities and differences between oceanic ridges and oceans. In order to do

62   this, a dual approach was wielded, assessing a short-term comparison between fauna and environment (23 days)

63   and a longer-term comparison of environmental variables (9 months) featuring the same observation window at

64   both study sites.

65

2. Material and Methods

2.1. Observatories and study sites

68   Two similar ecological observatory modules, called TEMPO and TEMPO-mini were deployed in two different

69   oceans in 2011 (Fig. 1). The first one (TEMPO) was part of the EMSO-Azores observatory (http://www.emso-

70   fr.org/EMSO-Azores) and was deployed on the Lucky Strike vent field on the Mid-Atlantic (MAR) Ridge, south

71   of the Azores. The wireless EMSO-Azores observatory consists of two main hubs, positioned east and west of the

72   central lava lake that is characteristic of the Lucky Strike vent field. The eastern hub (Seamon East, Blandin et al.,

73   2010) focuses on hydrothermal vent ecology and hosts the TEMPO module. TEMPO was positioned at the

74   southern base of the hydrothermally active Eiffel Tower edifice at 1694 m depth. Its counterpart, TEMPO-mini,

75   was implemented on the region-scaled cabled network NEPTUNE (http://www.oceannetworks.ca/) in the North-

76   East Pacific (NEP), as part of the Endeavour instrument node. It was deployed at the Grotto hydrothermal vent at

77   a depth of 2168 m at Main Endeavour Field (MEF). Both modules were equipped with a video camera, temperature

78   probes, a CHEMINI Fe analyser (Vuillemin et al. 2009) and an optode measuring temperature and oxygen. An

79   additional instrument measuring turbidity was deployed in the vicinity of the TEMPO module in 2011 (Table 1).

80   The biggest discrepancy between both modules was the energy provision, with the Atlantic one (TEMPO) being
81   autonomous and battery-dependent (wireless), and the North-East Pacific one (TEMPO-mini) being connected to
82   a cabled network. Detailed descriptions of both modules can be found in Sarrazin et al. (2007; 2014) for TEMPO
83   and Auffret et al. (2009) and Cuvelier et al. (2014) for TEMPO-mini.
84
85   Henceforth, the Atlantic set-up (TEMPO on MoMAR/EMSO-Azores) will be referred to as MAR, and the North-
86   East Pacific (TEMPO-mini on NEPTUNE/ONC) set-up as NEP (Fig. 1).
87

88   **2.2. Data collection and recordings**

89   Data collected consisted of video imagery recordings, temperature measurements, iron and oxygen concentrations,
90   and turbidity measurements (the latter for MAR only) (Table 1), which were recorded jointly for the period 7-30
91   October 2011. Differences in recording resolutions were mainly due to different observatory set-ups and more
92   particularly due to the cabled or wireless network characteristics and their inherent energy limitations (continuous
93   power vs. battery dependence). On NEP, TEMPO-mini was equipped with a thermistor array of which two probes
94   (T602 and T603) were deployed on an assemblage most similar to the one filmed (see Cuvelier et al., 2014).
95   Therefore, only those two probes were used in the comparison to the MAR temperature data, which was recorded
96   directly on the filmed assemblage.
97

98   Iron concentrations (Fe) were measured on top of the assemblage and within the field of view (FOV) on the MAR
99   (Laës-Huon et al., 2015; Sarradin et al., 2015) and below the FOV on the NEP. An *in situ* calibration was performed
100   at NEP, analysing 2 Fe standards a day of 20 and 60 μmol/l; no such calibration took place at the MAR. At NEP,
101   sampling frequency was changed from twice (30 September 2011 to 18 October 2011) to once a day (19 October
102   2011 to 31 January 2012) due to rapidly decreasing reagents. Fe concentrations were analysed for the longer-term
103   and used to explore the differences between the observatory settings.
104

105   Closer examination of data recorded by the optode revealed some inconsistencies between the measured
106   temperature and the O_2 concentrations. As the O_2 concentrations were corrected by the temperature, a difference
107   in the response time between the temperature and oxygen sensor within the same instrument was presumed. This
108   lag could not be quantified, making comparisons with other observations impossible. Oxygen concentrations
109   measured were thus merely used as illustration to compare the differences between the two hydrothermal settings.
110

111   Turbidity was only measured at the MAR observatory in Nephelometric Turbidity Units (NTU), which were
112   straightforward in their interpretation, i.e. the higher the more turbid. The sensor is not calibrated as such as its
113   response depends on the particle size, which was unknown. Hence it only provided information on the relative
114   turbidity (and peaks) of the environment.
115

2.3 Short-term temporal analyses

A unique subset of comparable data, allowing a joint assessment of faunal densities and links with the environment, was available for the time period 7-30 October 2011 for both observatories. The image analysis period was limited because of data availability, which in this case was restricted by the imagery recordings from NEP, spanning 23 days (see Cuvelier et al. 2014).

2.3.1. Imagery analysis

The variations occurring in the faunal assemblages in the two hydrothermal vent settings were analysed for 23 days with a 6h frequency (at 0h, 6h, 12h, 18h UTC). Due to gaps in the data recordings different number of images were analysed for MAR and NEP (Table 2).

The surface filmed by each observatory was different, which is why densities (individuals/m^2) were used instead of abundances. In each setting, there was also a discrepancy between the surface filmed and that analysed (Table 2, Fig. 2). Some surfaces were not taken into account because of their increased distance to the camera and the focal point, or due to the probe positioning within the FOV, making it impossible to quantify the fauna. These surfaces are marked in black and white on the sketch in Fig. 2. Both sketches were made based on a composed image, i.e. a merge of all images analysed, hence showing the most recurrent species distributions. For MAR, main shrimp cluster/distribution was confirmed using Matabos et al. (2015). For NEP, heat maps from Cuvelier et al. (2014) were used to confirm and localise mobile fauna. This does not mean that the mobile fauna does not venture elsewhere, but it showed an average distribution.

The Atlantic and Pacific oceans feature distinct hydrothermal vent fauna and while they do share several higher-level taxa, most species are different for the two oceans (Fig. 1 and 2). The main visible species and engineering taxon present for the 'shallower' (<2300m) MAR vents is a mytilid (*Bathymodiolus azoricus*) versus a siboglinid tubeworm for the NEP (*Ridgeia piscesae*). The second most characteristic Atlantic taxon is the *Mirocaris fortunata* alvinocaridid shrimp (Desbruyères et al., 2001; Cuvelier et al., 2009). Contrastingly, no hydrothermal shrimp are present at NEP vents, but associated visible fauna consisted of Buccinidae (Gastropoda), Polynoidae (Polychaeta) and Pycnogonida (containing the family Ammotheidae) (Cuvelier et al., 2014; Table 2, Fig. 2). The latter two taxa were also present at the shallower MAR sites as well as a bucciniform gastropod (Turridae family), be it in lower abundances and represented by different genera and species. In the Atlantic field of view, a small patch of anemones (Actiniaria) was visible below the probe as well.

Overall, imagery analysis was limited to the abundance assessment of the visible species (Cuvelier et al., 2012). In this perspective, tubeworm densities corresponded to the number of visible tubeworms, i.e. those that had their branchial plumes out of their tube at the moment of the image analysis. Stacked limpets were visible on the NEP imagery but were impossible to assess quantitatively due to their small size and piling (Cuvelier et al., 2014). Coverage of microbial mats was analysed on a 12h frequency at both sites.

2.3.2. Environmental data

An active fluid exit was visible on the images of the MAR, but not on the NEP recordings. The probe measuring the MAR environmental variables was positioned next to this fluid exit in the FOV, whilst the different probes of NEP (multiple probes measuring different environmental variables, see *in situ* observatory set-up in Cuvelier et al., 2014) were deployed below the FOV. The frequencies with which the environmental variables were recorded are listed in Table 1. Due to the large variability and steep gradients in environmental conditions observed at the hydrothermal vent ecosystems, the temperature variables used in the analyses were averaged per hour to reduce noise and variance. For those variables used as explanatory variable (temperature and turbidity) in the joint analyses with the available faunal densities, every 6th h value was taken (corresponding with the 6h frequency at 0h, 6h, 12h and 18h UTC). Only probes T602-T603 from NEP were used for comparison with MAR. The R package hydroTSM (Zambrano-Bigiarini M., 2012) was used to create an overview of the variations of hourly temperature values during imagery duration.

Fe was only sampled with a 12h or 24h frequency, hence limiting its use as an explanatory variable for the higher resolution faunal dynamics.

2.3.3. Statistical analyses

Multivariate regression trees (MRT, De'ath, 2002) were computed on Hellinger-transformed faunal densities. This analysis is a partitioning method of the species density matrix of each observatory, constrained by time. It grouped consistent temporal observations and thus identified groups with similar faunal composition that are adjacent in time; these groups are called "temporal split groups" from here on. Each split is chosen to maximise the among-group sum-of-squares and the number of split groups is decided upon by choosing the tree with the lowest cross-validation error; that tree has the best predictive power. For this type of analysis, the observations do not need to be equi-spaced, as long as the constraining variable reflects the sampling time (Legendre & Legendre, 2012). The MRT partition was then subjected to a search for indicator taxa (IndVal analysis, Dufrêne & Legendre, 1997; function multipatt() in R package Indicspecies (De Caceres & Legendre, 2009)). The IndVal index combines a measure of taxon specificity with a measure of fidelity to a group and thus reveals which taxon was significantly more or less abundant in the group before than after the split. Its significance is assessed *a posteriori* through a permutation test (Borcard et al., 2011). The observed temporally consistent groups were delineated by colour-codes within a Redundancy Analysis (RDA) ordination plot; RDA's were carried out on Hellinger transformed faunal densities and environmental variables to visualise the possible influence of the environmental constraints on the temporal groups found in the faunal density matrices.

Rhythms and periodicities in faunal densities and environmental variables were examined with Whittaker-Robinson (WR) periodograms (Legendre 2012). These WR periodograms were computed on the faunal densities, with a 6h resolution, and on the environmental variables with an hourly resolution (see 2.4). Prior to these analyses, stationarity was implemented by detrending time series when necessary. Time series were folded into Buys-Ballot tables with periods of 2 to a maximum of n/2 observations. The WR amplitude statistic was the standard deviation of the means of the columns of the Buys-Ballot table. Missing values were taken into account and filled in by NA values (''Not Available'').

193 In order to establish differences or similarities in the variations observed in temperature data from MAR and NEP,
194 cross-correlations were carried out on the hourly temperature data for imagery duration (n=553). Cross-
195 correlations could not be carried out between faunal and environmental variables, because the time series were
196 relatively short and they contained gaps, an irregularity which cross-correlations cannot take into account.

197

198 No specific correlations between faunal densities and environmental variables were presented since to the high
199 spatial variation and the locality of NEP probes on the one hand and the relatively large surface filmed in the MAR
200 setting on the other considerably decreased representativeness. Structuring strength and tendencies of
201 environmental variables in faunal composition were deduced from ordinations.

2.4 Long-term temporal analyses

203 For the time period 29 September 2011 to 19 June 2012, environmental data spanning 9 months featuring
204 temperature and iron were available for compared analyses, turbidity was only available for the MAR. The oxygen
205 time series revealed the issues explained previously (see 2.2), hence they were not subject to temporal analyses
206 but the differences in concentrations measured between the two observatory locations were addressed. Faunal
207 densities could not be assessed on the longer term due to the lack of regular imagery recordings for MAR and NEP
208 but also changes in zoom and subsequently image quality for the NEP. Long-term time series analyses in the form
209 of WR periodograms were carried out on the hourly data for temperature and turbidity, and daily/12h (NEP/MAR
210 respectively) frequency for Fe to allow comparison between MAR and NEP. See section 2.3.3 for details on the
211 periodogram analyses.

3. Results

3.1. Short-term variability

3.1.1. Fauna

215   **MAR** – In total, 84 images were analysed from the TEMPO module; there were 9 gaps in the imagery data
216 series (Table 2). The most abundant visible species were *Bathymodiolus azoricus* mussels and *Mirocaris fortunata*
217 shrimp, the numbers of the other taxa (crabs, polynoids, bucciniform gastropods, pycnogonids) being an order of
218 magnitude smaller (hundreds vs. single occurrences, for densities see Fig. 3.). An overall significant increase in
219 mussel and shrimp densities was observed (R^2=0.68, p-value<0.001 and R^2=0.32, p-value<0.001 respectively, Fig.
220 3). Conversely, a significant negative trend was observed for the bucciniform gastropods (R^2=0.19, p-value<0.001,
221 Fig. 3). For the other taxa, no significant trends in densities were observed. Trends were removed prior to
222 periodogram analyses, which revealed no significant rhythms in mussels, shrimp, crabs and bucciniform
223 gastropods. Only for polynoid scale worms, a significant 18 h period was observed, followed by significant periods
224 at 90 h (3.75 days or 5*18 h), 186 h (7.75 days or ~10*18 h) and 204 h (8.5 days or ~11*18 h) (Fig. S1). Polynoids
225 were mostly found on bare substratum though they ventured on the mussel bed occasionally. In fact, 92% of the
226 observations were associated with bare substratum vs. 8% observations on the mussel bed. One large individual
227 occupied the exact same area in 61% of all images analysed (Fig. 2). Bucciniform gastropods were observed on
228 the bare rock in the foreground further away from the fluid exit (Fig. 2). Pycnogonids (7 observations) and the
229 occasional ophiuroid (4 observations) were observed mostly at the edge or on top of the mussel bed, further away

230   from fluid flow. *Segonzacia mesatlantica* crabs were mobile, some moving in the FOV, others appearing between

231   the mussels. Their distribution was rather heterogeneous but mostly associated with the mussel beds and shrimp

232   presence. A *Cataetyx laticeps* fish was observed 5 times within the analysed time series – mostly in the background

233   and not interacting actively with the other organisms. Its presence was only discernible based on the video footage

234   (and not on the screen stills). The small patch of anemones observed below the probe featured 33 individuals. No

235   changes were documented over time for this taxon.

236

237   **NEP** – 88 images were analysed from the TEMPO-mini module; the dataset featuring 5 gaps (Table 2). *Ridgeia*

238   *piscesae* tubeworms were the most abundant taxon assessed on imagery, adding up to several hundred visible

239   (outside their tubes) individuals and providing a secondary surface for the other organisms to occupy. Thus, several

240   dozens of pycnogonids, up to a dozen of polynoids and a couple of buccinids were present on the tubeworm bush

241   (for densities see Fig. 3.). The strings of stacked limpets were not quantified. Only pycnogonid densities showed

242   a significant positive temporal trend (R^2=0.23, p-value<0.001, Fig. 3). For the other taxa, no significant trends

243   were observed. Periodogram analyses carried out on the faunal densities with a 6h period revealed a distinct 12h

244   frequency and harmonics for tubeworms, a single 12h period (i.e. no harmonics) and 222h (9.25 days) for

245   polynoids (Fig. S2). Buccinids also showed some significant frequencies at 174h (7.25 days) and 204-228h (~8.8

246   days, Fig. S2), while none were observed for pycnogonids. All associated species (except for visiting fish) were

247   found on the tubeworm bush surface (see Fig. 2). Pycnogonids showed distinct clustering behaviour and spatial

248   segregation which were also observed, be it to a lesser extent, for the other taxa (buccinids and polynoids). 8 visits

249   of a *Pachycara* sp. (Zoarcidae) were documented, during which the fish was present next to the tubeworm bush

250   and sometimes hiding underneath it. No specific behaviour of the fish interfering with the fauna of the tubeworm

251   bush was documented.

252

253   **Temporal split groups** - Different adjacent temporal groups were identified for MAR and NEP based on changes

254   in faunal composition and densities over time through Multivariate Regression Trees (MRT). Five temporal groups

255   were delineated for NEP and MAR (Table 3) though they were partitioned differently over time. Most groups

256   could be considered rather similar in time span for the two locations. For the MAR, the highest variance was

257   described by the split separating <195h and ≥195h. This coincided with an increase in shrimp and mussel densities

258   and decrease in gastropods and crab densities (Fig. 3), which were shown to be significantly indicative for different

259   split groups post-195h. Shrimp were found to be most indicative for the ≥321h group (IndVal=0.47, p=0.037) and

260   bucciniform gastropods for the ≥195h - <321h group (IndVal =0.78, p=0.0002). *Bathymodiolus* mussels were

261   indicative for the <51h group (IndVal =0.45, p=0.042) featuring the lowest densities for the studied time series.

262   Contrastingly for the NEP, splits coincided with the chronology and tubeworm densities were significantly

263   indicative for the <45h group (IndVal =0.46, p=0.001). Pycnogonids and buccinids were both indicative of ≥504h

264   (IndVal=0.51, p=0.0001 and IndVal=0.52, p=0.0013 respectively). The temporal split groups (Table 3) were

265   delineated onto the faunal variation graphs (Fig. 3) and used to colour-code groups in the ordinations in order to

266   investigate how individual taxa and environmental conditions coincide with and influence the temporal

267   inconsistencies represented by the MRT groups.

268

269   **Microbial Cover** - Despite the large difference in percentage of the image covered by microbial mats between

270 MAR (1.34 – 2.76%) and NEP (25.11 – 37.02%), both showed a decline during the period analysed (Fig. 4). The

271 observed trends were significantly negative for both sites. For the MAR, this decline resulted in a significant

272 negative correlation between microbial cover and mussel densities (r=-0.67, p=0.00) on the one hand and shrimp

273 densities on the other (r=-0.53, p=0.0004). For the NEP, no significant correlations between microbial cover and

274 other taxa were revealed.

275

276 **3.1.2. Environmental data**

277 Environmental data analysis presented in this section is a short-term analysis, spanning 23 days corresponding to

278 the imagery duration.

279

280 **Temperature -** Generally, higher temperatures were recorded at the MAR (Fig. 5). Mean temperatures at MAR

281 were higher than maxima recorded by probes T602 and T603 at NEP (Table 4), coinciding with higher ambient

282 seawater temperatures for the MAR (~4°C) than for NEP (~2°C). Even when rescaling to ambient temperature,

283 minimum temperatures measured on the MAR were still higher than those of the NEP. However, maximum and

284 mean temperatures no longer stood out and were even lower than those measured by probes T602 and T603 in the

285 NEP (Table 4). Standard deviations and variance were maintained and were consistently higher at NEP.

286

287 The hourly temperature recordings showed noticeable cycles of higher and lower temperatures specifically in T602

288 and T603 (which are visible as red and blue colours in Fig. 6 respectively). When such (more or less) coherent

289 bands of lower and higher values are observed in tidal pressure heat-maps, it shows the cyclical nature of the tides.

290 Hence, alongside the tidal rhythms revealed by the periodogram analyses, a tidal cyclicity was recognisable in the

291 temperature recordings of the NEP. Patterns were less clear for the MAR. Information on pressure data from the

292 same localities and correspondence to the temperature measurements was included as appendix/supplementary

293 material (Fig S3).

294

295 In order to investigate how the temperature time series from the two oceans relate to one another, cross-correlations

296 were carried out on the hourly temperature values (Fig. 7). Generally, positive autocorrelations were more

297 pronounced, meaning that the two series were in phase. Maximum autocorrelation was reached at lag +5 h when

298 comparing MAR to T602 with the MAR time series leading, and a +5 to +6 h lag between MAR and T603. Most

299 of the dominant cross-correlations occurred between lags +4 and +7, with tapering occurring in both directions

300 from that peak. This corresponds to the time difference of ~6h between MAR and NEP locations, calculated as

301 follows: 24*degrees (difference in longitude)/360. Maximum negative autocorrelations were observed at lags –14

302 and +11 for NEP T602 and MAR and between lags +10 and +13 for NEP T603 and MAR. The difference between

303 the maxima (and minima) closely corresponded to the tidal cycle (~6h).

304

305 **Fe –** There is a lag of 6 hours' time difference in the Fe-recordings carried out in the NEP being measured at 6 and

306 18h UTC and on the MAR at 12h and 0h UTC. Fe on the MAR was recorded twice a day (in 4 cycles) during the

307 analysed imagery period. Concentrations ranged from 0.41 µmol/l to 1.62 µmol/l with a mean of 0.81±0.28 µmol/l.

308 A non-significant (p=0.479) positive trend was observed but no significant relationships between fauna, microbial

309   cover and Fe were revealed. Fe measurements at NEP were limited to 7 days at a frequency of one measurement

310   a day. Consequently, its use as an explanatory variable for faunal variations was limited and no patterns were

311   revealed. Values ranged from 2.07 to 2.99 µmol/l, which were higher than those observed on the MAR but also

312   showed less variation.

313

314   **Turbidity** – Turbidity measurements (NTU) were restricted to the MAR observatory and a non-significant positive

315   trend was observed during imagery duration. A large peak was noticeable at ~400 h (around 23 October 2011)

316   though it was not reflected in any of the other environmental variables or community dynamics (Fig. 5).

317

318   **3.1.3. Fauna-environment interaction**

319   **MAR -** Environmental variables incorporated in the ordination analyses did not distinguish significantly between

320   faunal densities or the temporal split groups found in the faunal composition (Fig. 8). The first axis was

321   significantly more important for the MAR RDA (83.76%), hence attributing a higher importance to the horizontal

322   spreading. This separation corresponded mostly with the separation of *Mirocaris* and *Bathymodiolus*. NTU seemed

323   to have a distinct impact on separating the images from one temporal split group (51h-159h), though there was no

324   clear signal in NTU values at that time. Overall, for the MAR, no distinct relationship between a specific taxon

325   and measured environmental variables was revealed.

326

327   **NEP -** The first axis of the NEP RDA also explained most of the variance (98.2%) represented by the ordination

328   plot (Fig. 8). This coincided with a separation in the plot between Pycnogonida, Polynoidae and Buccinidae that

329   pooled apart from the tubeworms. This lateral separation in taxa coincided with the strong correlation between

330   tubeworm densities (appearances) and the T602 and T603 temperature measurements. Temporal split groups were

331   vertically aligned in the plot and tended to overlap, with tubeworms being more indicative for <45h group (as

332   corroborated by the "multipatt indval" analysis). No clear influence from the environmental variables on the

333   separation in temporal split groups could be revealed.

334

335   **3.2. Long-term variability**

336   Long-term variations in environmental conditions from both observatories spanning 9 months were investigated.

337   The long-term time series analysed was limited by the shortest deployment period for which both observatories

338   were up and running at the same time. Long-term analysis was thus restricted by the TEMPO-mini observatory

339   (NEP), whose deployment spanned ~9 months (29 September 2011– 20 June 2012).

340

341   **Temperature**

342   The continuous MAR temperature time series showed temperature variations between 4.48 and 10.91°C, with a

343   mean of 5.54 ± 0.71 °C (Fig. 9). A significant negative trend in temperature values was observed over the 9-month

344   period. This negative trend was already visible in the short-term analyses as well. The NEP temperature values

345   recorded during this period by T602 and T603 were comprised between 2.23°C and 5.43°C, with a mean of 3.78

346   ± 0.54°C. T602 showed a significant negative trend (p<0.001) while T603 showed a significant positive trend

347   (p<0.001) over the longer term. Trends were removed and periodogram analysis was carried out on the residuals

348   for periods of 2 to n/2 (3168 h ~ 4.5 months), 2 to 800 h (~1 month), and 1 week periods (2 to 200 h). Regardless

349   of the time-span, diurnal and semi-diurnal periods and their harmonics were the main significant frequencies

350   discerned. No clear or distinct significant hebdomadal (weekly) or infradian (multiple days) cycles were

351   encountered. Therefore, in order to facilitate interpretation, only the periodograms with periods of 2 to 200 h are

352   presented (Fig. 10).

353

354   A significant period at 12h was revealed for the MAR and NEP T602 probes, but not for T603. For T603, a peak

355   was present at T=12h but it was not significant; however, harmonics of that peak at 25, 37, 50 and 74, 75h (etc.)

356   were significant. A significant 25h period was thus observed for both NEP probes (T602 and T603). Recurrent

357   harmonics of both semi-diurnal (12h) and diurnal (25h) frequencies were identifiable throughout the temperature

358   time series, more so for NEP time series than for MAR, which agree well with the tidal cycle (12h 25 min and 24h

359   50 min) (Fig. 10). A distinct 6.25-day period (at 150h) with a high amplitude was revealed for the T602 and T603

360   probes (Fig. 10). Such a peak was recognizable for the MAR as well, though it was not significant. A peak at 174h

361   (7.25 days) was significant for all three probes (MAR & NEP). The corresponding significant periods between

362   MAR and NEP were thus 12h, 37h, 87h, 112h and 174h though some were less pronounced depending on the

363   ocean.

364

365   **Fe**

366   A negative almost significant trend (p=0.053) was observed for 6 months of data (30 Sept 2011 to 29 March 2012)

367   from the MAR featuring two Fe measurements a day (at 0 and 12 UTC) (Fig. 9). Minimum and maximum

368   concentrations were 0.25 and 2.61 µmol/l respectively with a mean at 0.98 ± 0.43 µmol/l, which was lower than

369   the averaged concentrations of the other deployment years (with 2.12 ± 2.66 µmol/l averaged over 2006, 2010-

370   2011, 2012-2013 and 2013-2014). Periodogram analyses revealed a peak at 108h (4.5 days) and a more pronounced

371   one at 180h (7.5 days), but none of these were significant. For the NEP, a time series of one Fe measurement a day

372   (at 6 AM UTC), consisting out of 4 sampling cycles, spanning >4 months was analysed (20 October 2011 – 26

373   March 2012). The last 49 (31 January 2012 – 26 March 2012) days were omitted due to artefacts visible in Fig. 9,

374   which was due to the reagents running down. Periodogram analysis of these ~3 months of data revealed no

375   significant periods either. Fe concentrations ranged from a minimum of 0.67 µmol/l to a maximum of 5.45 µmol/l;

376   with mean values at 2.40 ± 1.03 µmol/l. Mean values approached the maximum values measured by the MAR

377   observatory, similar to what was observed in the short-term analyses.

378

379   **Oxygen**

380   Due to the unresolved issues with the optodes and the oxygen concentrations measured (see section 2.2) the

381   absolute values were taken into account, however the differences in overall concentration were used to describe

382   the differences between the two sites. For the MAR, measurements ranged from 170.54 to 251.66 µmol/l with

383   mean 230.62 ± 16.98 µmol/l. The NEP featured distinctly lower concentrations, ranging from 23.67 µmol/l to

384   77.26 µmol/l with a mean of 63.42 ± 7.15 µmol/l. Here as well, there seemed to be more variablity at the NEP

385   than at the MAR.

386

387 **Turbidity**

388 Turbidity was only measured at the MAR observatory and showed several large peaks further along in the long-
389 term time series (e.g. during end February 2012 and May to June 2012) (Fig. 9), however none of these
390 observations translated themselves in the other environmental variables. There was a significant positive trend for
391 NTU over 9 months (p<0.001) but no significant periods were revealed by the periodogram analyses.

392 **4. Discussion**

393 **4.1. Faunal assemblages**

394 Vent fauna hosted by the two study sites are quite different. While there are similarities at higher taxonomic levels,
395 e.g. classes and families, there is only one correspondence on genus level (*Sericosura* sp., Pycnogonida) and none
396 on species level between both sites. A higher number of visible taxa were identified on MAR images when
397 compared to NEP (8 vs. 6, respectively, not taking into account microbial cover or visiting fish species). This
398 observation does not imply that the MAR is more diverse than the NEP since imagery only gives a partial overview
399 of the actual diversity (Cuvelier et al., 2012). In the subsequent sections temporal variations and behaviour
400 (rhythms) of the separate taxa and their implications for possible microhabitat and niche occupation will be
401 discussed.

402 **4.1.1. Engineering species**

403 MAR – *Bathymodiolus azoricus* mussels visually dominate the shallow water (<2300m) vents along the MAR and
404 appear to be a climax community, being present for a few decades on the same edifices within the Lucky Strike
405 vent field (Cuvelier et al., 2011b). They form dense faunal assemblages in relatively low temperature microhabitats
406 (Cuvelier et al., 2011a; De Busserolles et al., 2009). Contrastingly to what has been described by Sarrazin et al
407 (2014) no significant interactions between mussels and other organisms could be revealed based on the 6h
408 frequency analysed here.

409

410 NEP – Tubeworms of the species *Ridgeia piscesae* were the main visible constituents of the filmed assemblage
411 and a secondary surface for the associated fauna assessed here. Their appearance rate showed a strong relationship
412 with the temperature recorded by probes T602 and T603 (Cuvelier et al., 2014 and this study), contrastingly to the
413 other taxa. Whilst interactions between tubeworms and other taxa were not significantly quantifiable on the current
414 6h frequency of image analyses, they have been observed and described for the hourly frequency (Cuvelier et al.,
415 2014).

416

417 **4.1.2. Shared taxonomic groups**

418 Polynoidae – Free-living MAR scale worms were preponderantly associated with bare substratum, while those
419 quantified for NEP were only those observed on top or within the tubeworm bush. They were also visible on the
420 bare substratum surrounding the tubeworm bush but this area that was not taken into account. While there was a
421 difference in substratum association between polynoids as observed by the two observatories, all individuals
422 seemed to be rather territorial (see Cuvelier at al., 2014). On the MAR, one individual appeared very attached to

423   one single area within the FOV, returning to it repeatedly after excursions. Such behaviour might be indicative of

424   topographic memory and homing behaviour. Many of the free-living polynoid species are known as active

425   predators (Desbruyères et al., 2006).

426

427   Gastropoda – Buccinid (NEP) and bucciniform (MAR) gastropods appeared more related to less active

428   environments. Within the MAR setting, snails (*Phymorhynchus* sp.) were present in very low abundances (1 or 2

429   individuals at most) and were positioned on bare rock with no fluid flow. In the NEP setting, whelks (*Buccinum*

430   *thermophilum*) were generally more abundant on to areas inhabited by vent animals. Numbers observed within the

431   FOV tended to vary from 1 to 6, while they were shown to congregate in groups of 5 or more individuals at MEF

432   (Martell et al., 2015). Both species were considered predators or scavengers (Desbruyères et al., 2006; Martell et

433   al., 2015).

434

435   Pycnogonida – Sea spiders showed a very distinct spatial distribution in NEP, whilst their presence on the MAR

436   was occasional. At the latter, individuals were observed visiting the edge of the mussel bed, further away from

437   venting. A large difference in pycnogonid densities was observed between the two sites as well, with a ratio of

438   1/250 MAR vs. NEP. Interestingly, these organisms all belong to the same genus, namely *Sericosura*. The species

439   known for the Lucky strike vent field (MAR) is *Sericosura heteroscela* while there are multiple species (within

440   the same genus) for the Main Endeavour Field (NEP) among which *Sericosura verenae*. All *Sericosura* species

441   from the Ammotheidae family known so far appear to be mostly obligate inhabitants of hydrothermal vents or

442   other chemosynthetic environments (Bamber, 2009). Based on their abundance or scarcity in the study sites, their

443   local niche occupation is likely to explain the discrepancy in densities observed between the studied sites.

444

445   Microbial cover – This is a generic term used to refer to the microbial mats colonising various surfaces in the vent

446   environment without assuming similar microbial composition. While no significant relationships were revealed

447   between microbial cover and fauna for NEP in the current study, a significant negative correlation was observed

448   for this site between pycnogonids and microbial cover based on the same imagery analysed with a higher frequency

449   (4h instead of 12h), which was attributed to pycnogonid grazing (Cuvelier et al. 2014). For MAR, significant

450   negative correlations existed between microbial coverage and mussels on one hand and shrimp on the other. For

451   the mussels, this could be due to scattering and repositioning of individual mussels: as mussel reposition on top of

452   the microbial mats, they decrease the visible and assessable microbial coverage. The negative relationship between

453   shrimp and microbial cover could be caused by the shrimp grazing on microorganisms (Gebruk et al., 2000; Colaço

454   et al., 2002; Matabos et al. 2015).

455

456   **4.1.3. Regional taxa**

457   **MAR**

458   Alvinocaridid shrimp – The hydrothermal shrimp observed by the MAR observatory mostly belong to the

459   *Mirocaris fortunata* species. On the images analysed, they were most abundant in the main axe of flux. Matabos

460   et al. (2015) quantified this to about 60% of the shrimp abundances (to 69cm of an emission), confirming previous

461   distributional patterns of shrimp being indicative of fluid exits and characteristic for warmer microhabitats

462   (Cuvelier et al., 2009, 2011; Sarrazin et al., 2015). Because their distribution is linked to the presence of fluid exits

463   and flow, a significant positive correlation between shrimp and temperature would be expected. To date however,

464   such a relationship could not be designated, not in this study or in previous studies based on data from the deep-

465   sea observatories (Sarrazin et al., 2014; Matabos et al., 2015), though Sarrazin et al. (2014) did show a significant

466   positive correlation between *Mirocaris fortunata* abundances and vent fluid flux.

467

468   Bythograeidae (Decapoda) – *Segonzacia mesatlantica* crabs were mostly associated with the mussel beds and

469   anhydrites, as where the shrimp (Matabos et al., 2015). Some interactions between crabs and shrimp were observed

470   mostly resulting in shrimp fleeing. Possible significance of these interactions (mostly territorial in nature) were

471   described in more detail by Matabos et al. (2015).

472

473   Bythitidae (Osteichthyes) - The fish *Cataetyx laticeps* was frequently observed at the base of the Eiffel Tower

474   edifice within the Lucky Strike vent field (Cuvelier et al., 2009). No feeding action on the benthic hydrothermal

475   fauna was observed during the 6h frequency image analyses.

476

477   **NEP**

478   Majidae (Decapoda) - Contrastingly to the 1h frequency observations (Cuvelier et al., 2014), no spider crabs were

479   observed visiting the filmed assemblage on a 6h frequency imagery analyses. Whilst this majid spider crab is

480   known as a major predator at hydrothermal vents, no such actions were recorded by the observatory.

481

482   Zoarcidae (Osteichthyes) – Similarly as for *Cataetyx* fish on the MAR, no visible activities of feeding or predation

483   of *Pachycara* sp. eelpouts were observed on the NEP. Cuvelier et al. (2014) proposed that the eelpouts (and fish

484   in general) may be more sensitive to the effects of lights but this hypothesis, based on behavioural observations,

485   could not be confirmed in the present study due to the low-resolution observation frequency.

486

487   **4.2. Behavioural rhythms and variations**

488   When looking at the engineering taxa for each ocean, a clear diurnal rhythm was observed in visible (i.e. out of

489   their tubes) tubeworms (NEP), while there was a lack of temporal rhythms in mussel densities (MAR). However,

490   taking in to account the characteristics of both chemosynthetic taxa, mussel valve openings instead of densities

491   should be used for comparison to tubeworms outside their tube. This difference in assessment could account for

492   the lack of temporal periodicities at the MAR, where mussel valve openings were impossible to quantify due to

493   the larger distance between the observatory and the filmed assemblage. Different causes might trigger a mussel to

494   open his valve or a tubeworm to come out of its tube and these can be either attributed to an external trigger (e.g.

495   retraction or closure after possible predation actions (for tubeworms: Cuvelier et al., 2014; for mussels: Sarrazin

496   et al., 2014) or to their physiology (need for nutrients or saturation). Until now, no significant links have been

497   established between fluid flow and open mussel valves (Sarrazin et al., 2014) but some indications of tidal

498   rhythmicity were visible (Matabos et al., unpublished data). No consistent statistically significant link between

499   fluid flow and tubeworm appearance has been revealed to date either (Cuvelier et al., 2014), although they showed

500   a steady significant semi-diurnal tidal rhythm over time. The niche occupation and role within the ecological

succession over time of mussels and tubeworms are very different for the two oceans. In Pacific monitoring studies, tubeworms were out-competed by mytilid mussels when hydrothermal flux started to wane (Hessler et al., 1985; Shank et al., 1998; Lutz et al., 2008; Nees et al., 2008), while the latter appear to represent a climax community in the Atlantic <2300m (Cuvelier et al., 2011b).

Next to the engineering species, only a few other taxa showed significant periodicities in densities over time, namely polynoids for MAR and NEP, and buccinids for NEP. The lack of significant periodicities in MAR shrimp was corroborated by a more long-term study by Matabos et al. (2015). Both polynoids and buccinids displayed multiple day periodicities instead of tidal cycles, which could be mostly reduced to harmonics of tidal cycles that become more visible further along in the time series as they get more pronounced over time. For both taxa, the multiple day periodicities revealed approached those visible in Fe, i.e. 4.5 and 7.5 days (though non-significant). More thorough and high resolution investigations will be necessary to corroborate or validate these observations. Overall, the reasons for the lack of periodicities in fauna can be twofold: either the taxon in question is unevenly represented in low abundances and therefore too heterogeneous (rendering any statistical test difficult which was the case for MAR crabs and pycnogonids) or the recording/analysing frequency does not allow discerning of significant periods. The shortest period to be resolved is twice the interval between the observations of a time series. Hence, caution is needed when interpreting patterns as the recording and/or analysing frequency influences observations. Moreover, it was shown previously in a higher resolution study (hourly frequencies) that depending on the frequencies investigated the type of relationships (significance, positive or negative) between the taxa might change (Cuvelier et al., 2014).

While certain environmental variables might explain a large amount of variation occurring in a single or specific taxon (e.g. NEP tubeworm appearances and temperature from probes T602 and T603), a wider variety of environmental variables measured at multiple sampling points in the FOV in a resolution similar or higher than the imagery analyses frequency should be considered in order to explain and comprehend the whole of community dynamics. This was also illustrated with the temporal split groups identified in community composition constrained by time, which were quite similar for the larger groups (those with higher n) with split groups at the MAR occurring 6 hours later than those at the NEP. A slower pace in significant detectable changes in overall faunal composition in the Atlantic vs. the NE Pacific could be explanatory. For instance, difference in spreading rate was shown to be directly proportional to different rates of change in community dynamics between slow-spreading MAR and faster-spreading NEP (Cuvelier et al., 2011b). However, for now, the predictive power of the split groups was rather low and groupings could not be corroborated with changes in the environmental variables.

4.3. Environmental rhythms and conditions

Highest minimum temperatures were recorded at the MAR where the probe was positioned closer to a visible fluid exit, whereas NEP temperatures were the most variable and displayed broadest ranges. It is important to bear in mind that ambient seawater temperature at 1700m on the MAR is higher than that at 2200m depth in the NEP (4°C vs. 2°C respectively). When taking this into account and rescaling the temperature values, mean and maximum temperatures were highest at NEP. Highest positive and significant autocorrelation values indicated a ~5-6h lag

540   between MAR and NEP, with MAR leading. Interestingly, the hour difference between the two sites corresponds

541   to ~6 hours as well. The geographical distance separating the two localities does thus not only allow to quantify

542   the time difference between two sites but also the delay in the tidal rhythms observed between the two.

543

544   Tidal rhythms were discernible in both NEP and MAR series. For NEP, diurnal periods at ~25 h were discerned

545   for both probes (T602 and T603). Significant semi-diurnal periods were also found in T602, though for T603 they

546   could only be identified based on their harmonics. Similarly, the MAR temperature time series had a

547   distinguishable semi-diurnal component.

548

549   Between oceans, there are differences in the observation of tidal rhythms based on the high (>200°C) and low

550   (<10°C) temperature records. For the NEP, the tidal influence appears to wane in high temperature records making

551   tidal signals less clear or even non-existent (Tivey et al., 2002; Hautala et al., 2012). While for the MAR the semi-

552   diurnal variability in the high temperature records was shown to be more significant and to be more coherent with

553   pressure than those observed in low-temperature (Barreyre et al., 2014). Unfortunately, we cannot corroborate this

554   with the current study as only low-temperature time series were recorded by both ecological observatories. Even

555   though we revealed some similarities in the rhythms of MAR and NEP low temperature series collected for the

556   same period, there are indications, that local hydrography controlling tides and associated bottom-currents play a

557   major role on the temporal variability of diffuse outflow and vent discharges (Barreyre et al., 2014, Lee et al.,

558   2015). Clear peaks in temperature variables were noticeable at ~6-7 days in MAR and NEP. We do not know what

559   caused this period to be significant. At Cleft Segment more southwards on the Juan de Fuca Ridge (NEP), Tivey

560   et al. (2002) found 4-5 day broadband peaks in temperature from diffuse flow as well as high-temperature vents

561   which were thought to be storm-induced from the sea-surface.

562

563   Fe (iron) - Fe is used as a proxy for vent fluid composition. Higher Fe concentrations would thus be expected

564   where temperatures were higher, in this case at MAR (vs. NEP). However, the opposite was observed here.

565   Moreover, the Fe concentrations reported here for the MAR in 2011 were lower than the Fe concentrations from

566   other deployment years at the same site (Laes-Huon et al., unpublished data). The 2011 concentrations recorded

567   at the MAR were really close to the detection limit of the CHEMINI instrument (0.3μmol/l). Additionally, the

568   MAR system was not calibrated *in situ*, contrastingly to the NEP, which could have generated a lower accuracy in

569   the calculated concentrations, though question remains if such large discrepancies can be explained by this feature.

570   The location of the sample inlet and the high spatial variation occurring at hydrothermal vents might contribute to

571   the patterns observed. The values observed at NEP, on the other hand, were in the same order of magnitude as

572   those reported for the Flow site also on the Juan de Fuca Ridge (i.e. 0 to 25 μmol/l, Tunnicliffe et al. (1997)). No

573   significant periods (based 12h or 24h recording frequency) were found for the duration of the deployment, although

574   some indications of 4.5 and 7.5 day periodicities could be observed at the MAR and 3.8 day cycles for Fe

575   concentrations were detected in the same sampling area for 2012-2013 (Laës-Huon et al., in press). For the North

576   East Pacific, 4 day oscillations in currents near seamounts along the crest of the Juan de Fuca Ridge were observed

577   (Cannon and Thomson, 1996), however, these were not visible in the Fe time series at NEP, although 4.5 day

578   periodicities were visible in buccinids and polynoids (Cuvelier et al., 2014). Hence, there were some indications

579 of multiple day periodicities, but these findings need to be corroborated, preferably by using a higher sampling

580 frequency.

581

582 Turbidity – NTU levels observed showed several large peaks over time. Particle flux at Lucky Strike combines

583 both large and small diameter particles which have different settling velocity (Khripounoff et al., 2000).

584 Kripounoff et al. (2008) showed an increased particle flux in April that reached a maximum end May (2002).

585 These do not correspond to the peaks observed here (in this study peaks were most pronounced at the end of

586 October, February to March and May to July) but turbidity peak occurrences tend to differ between years and

587 seasons. Due to seasonal peaks, longer time series will be needed to reveal recurrent patterns.

588

589 Generally, multiple day periodicities are harder to reveal as many of them can be reduced to harmonics of the tidal

590 cycles. In this perspective, the long(er)-term environmental variable analyses were considered more robust due to

591 increased number of data points. Nevertheless, there is not much we can currently say on multiple day or

592 hebdomadal cycles observed in the time series presented here.

593 **4.4. Limitations**

594 Overall, it remains hard to establish relationships among the environmental variables measured *in situ*. Ratios of

595 temperature to chemical concentrations are not constant, and can vary between sites (Le Bris et al., 2006; Luther

596 et al., 2012). There is also the issue of high variance (and noise) in environmental variable time series as well as

597 that of a possible delay in appearance of certain peaks, which makes it difficult to unravel patterns. Such a delay

598 between environmental variable recordings might exclude the ability of unravelling/exposing correlations. The

599 example for Fe and temperature recordings, where a delay of 1 to 5 min precluded a direct correlation for each

600 sample point, was presented by Laes-Huon et al. (2016).

601

602 Caution is needed when programming the recording frequencies of imagery and environmental variables. Despite

603 being mainly restricted by battery life (wireless observatories), light usage (wired observatories) or quantity of

604 reagents (both), a 6h analysing frequency might not be the most representative to assess faunal variations and links

605 with the environment. Indicative of this are the differences observed when analysing different frequencies as

606 briefly touched upon in Cuvelier et al. (2014) and comparing them with those presented here. It still proves difficult

607 to link faunal variations with the environmental variables measured *in situ*. This can either be due to the high

608 spatial and temporal variation of the environmental gradients compared to the larger FOV assessed or due to

609 recording frequencies or complexity of *in situ* measurements with corrections to be applied and possible delays.

610 Temperature still seems the best proxy for faunal variations, however not all faunal presence/absence, abundances

611 or the entirety of community dynamics can be explained solely by temperature. Biotic interactions are at play as

612 well, which can be observed thanks to the remote observatory set-up granting us access to long-term high

613 resolution data, but these may change as well according to local environmental conditions, gradients and harshness

614 (Mullineaux et al 2003).

615

616   Deployment of probes has also proven to be a predicament. While more accessible sites tend to be preferred and
617   selected, deployment setting, accessibility, underwater conditions (e.g. currents), ROV manoeuvrability and skills
618   also influence the final observatory set-up.

619   **5. Conclusions**

620   Influence of the tides is visible in both settings, most clearly in temperature variables and in tubeworms
621   appearances. The geographical distance separating the two localities was shown to not only quantify the time
622   difference between two sites but also the delay in the tidal rhythms observed in temperature values (which is at a
623   ~6h lag) between the MAR and NEP. Temporal split groups in community composition are rather similar between
624   both settings, though the 6h delay is visible as well. Shared taxa comprised one genus (*Sericosura*), one family
625   (Polynoidae) and one class (a buccinid and a bucciniform Gastropoda) and based on their relative abundance and
626   behaviour, they seem to occupy different niches at the different hydrothermal vents. Nevertheless, it remains
627   complicated to unravel links with environment and to discern which environmental variable is the most influential
628   or explanatory. To date, temperature remains the most explanatory, though it cannot explain the entirety of
629   community dynamics. This is mainly due to the high spatial variation at hydrothermal vents and the single point
630   measurements done by the temperature probes. There thus remains a persistent need for more complementary and
631   representative data, measured at frequencies similar or higher than the imagery recordings and measured at
632   multiple points in the FOV. Recording frequencies are crucial: a 6h recording frequency might not be good enough
633   to represent the *in situ* reality. Also the implementations of instruments that do not imply complex tools but allow
634   the assessment of additional environmental variables (e.g. current meters) could be a way forward. (Semi-)
635   automated tools need to be developed for specific taxa and settings to assist in assessing faunal abundances on
636   images.
637

638   **Acknowledgments**
639   We thank the captains and crews of the R/V Pourquoi pas? and the R/V Thomas G. Thompson for their steadfast
640   collaboration in the success of the MoMARSAT and Neptune Ocean Networks Canada cruises. We are grateful to
641   the Victor6000 and ROPOS ROV pilots for their patience and constant support. The authors would like to thank
642   the LEP technical team for its valuable help both at sea and in the lab, the TEMPO and TEMPO-mini engineers
643   and technicians who developed and maintained the modules and the Ocean Networks Canada scientists and
644   engineers, whose engagement and professionalism made this study possible. DC is supported by a post-doctoral
645   scholarship (SFRH/BPD/110278/2015) from FCT and this study had also the support of Fundação para a Ciência
646   e Tecnologia (FCT), through the strategic project UID/MAR/04292/2013 granted to MARE. Thanks to IMAR for
647   support to DC during the preparation of this manuscript. This project is part of the EMSO-Açores research
648   program that benefited from an ANR research grant (ANR LuckyScales, ANR-14-CE02-0008).
649

650   **References**

651   Aguzzi, J., Costa, C., Furushima, Y., Chiesa, J., Company, J.B., Menesatti, P., Iwase, R., Fujiwara, Y. (2010)
652   Behavioral rhythms of hydrocarbon seep fauna in relation to internal tides. Mar. Ecol. Prog. Ser., 418: 47–56.
653

654 Auffret, Y., Sarrazin, J., Coail, J.Y., Delauney, L., Legrand, J., Dupont, J., Dussud, L., Guyader, G., Ferrant, A.,
655 Barbot, S., Laes, A., Bucas, K. (2009). TEMPOMini: a custom-designed instrument for real-time monitoring of
656 hydrothermal vent ecosystems. Martech 2009 conference proceedings.

658 Bamber, R.N. (2009). Two new species of *Sericosura* Fry & Hedgpeth, 1969 (Arthropoda: Pycnogonida:
659 Ammotheidae), and a reassessment of the genus. Zootaxa 68: 56–68.

661 Barreyre, T., Escartín, J., Sohn, R.A., Cannat, M., Ballu V., Crawford W.C. (2014). Temporal variability and
662 tidal modulation of hydrothermal exit-fluid temperatures at the Lucky Strike deep-sea vent field, Mid-Atlantic
663 Ridge. Journal of Geophysical Research: Solid Earth. 119(4):2543-66.

665 Blandin, J., Colaço, A., Legrand, J., Cannat, M., Sarradin, P. M., Sarrazin, J., 2010. The MoMAR D project : a
666 challenge to monitor in real time the Lucky Strike hydrothermal vent field. ICES J. Mar. Sci. 68, 416–424.

668 Borcard, D., Gillet, F., Legendre, P., (2011). Numerical ecology with R. Use R! series, Springer Science, New
669 York. p. 306

671 Cannon, G. A., Thomson, R. E. (1996). Characteristics of 4-day oscillations trapped by the Juan de Fuca Ridge.
672 Geophys. Res. Lett., 23 (13), 1613–1616

674 Colaço, A., Dehairs, F., Desbruyères, D., LeBris, N., Sarradin, P.M. (2002). δ13C signature of hydrothermal
675 mussels is related with the end-member fluid concentrations of H2S and CH4 at the Mid-Atlantic Ridge
676 hydrothermal vent fields. Cah. Biol. Mar. 43,259–262.

678 Cuvelier, D., Sarrazin, J., Colaço, A., Copley, J., Desbruyères, D., Glover, A. G., Tyler, P., Serrão Santos R.
679 (2009). Distribution and spatial variation of hydrothermal faunal assemblages at Lucky Strike (Mid-AtlanticRidge)
680 revealed by high-resolution video image analysis. Deep-Sea Res. Part I Oceanogr. Res. Pap.56, 2026–2040.
681 http://dx.doi.org/10.1016/j.dsr.2009.06.006.

683 Cuvelier, D., Sarradin, P. M., Sarrazin, J., Colaço, A., Copley, J. T., Desbruyères, D., Glover, A. G., Santos, R.S.,
684 Tyler, P. A. (2011a). Hydrothermal faunal assemblages and habitat characterisation at the Eiffel Tower edifice
685 (Lucky Strike, Mid Atlantic Ridge). Mar. Ecol. 32, 243–255.

687 Cuvelier, D., Sarrazin, J., Colaço, A., Copley, J. T., Glover, A. G., Tyler, P. A., Serrão Santos, R., Desbruyères,
688 D., (2011). Community dynamics over 14 years at the Eiffel Tower hydrothermal edifice on the Mid-Atlantic
689 Ridge. Limn Oceanogr. 56(5), 1624–1640

691 Cuvelier, D., de Busserolles, F., Lavaud, R., Floc'h, E., Fabri, M.-C., Sarradin, P.-M., Sarrazin, J. (2012).
692 Biological data extraction from imagery - How far can we go? A case study from the Mid-Atlantic Ridge. Mar
693 Env Res 82: 15–27.

695 Cuvelier, D., Legendre, P., Laes, A., Sarradin, P.-M., Sarrazin, J. (2014). Rhythms and community dynamics of a
696 hydrothermal tubeworm assemblage at main Endeavour field – a multidisciplinary deep-sea observatory approach.
697 PLoSOne 9, e96924.

699 Desbruyères, D., Segonzac, M. and Bright, M. eds., 2006. Handbook of deep-sea hydrothermal vent fauna. Pp.
700 544

702 De Busserolles, F., Sarrazin, J., Gauthier, O., Gélinas, Y., Fabri, M. C., Sarradin, P. M., Desbruyères, D. (2009).
703 Are spatial variations in the diets of hydrothermal fauna linked to local environmental conditions? Deep-Sea
704 Res. Part II Top. Stud. Oceanogr. 56, 1649–1664.

706 De Caceres, M., Legendre, P. (2009). Associations between species and groups of sites: indices and statistical
707 inference. Ecology, URL:http://sites.google.com/site/miqueldecaceres/

709 De'Ath, G. (2002). Multivariate regression trees: a new technique for modeling species–environment relationships.
710 Ecology. 83(4):1105-17.
711

712 Desbruyères, D., Biscoito, M., Caprais, J.C., Colaço, A., Comtet, T., Crassous, P., Fouquet, Y., Khripounoff, A.,
713 Le Bris, N., Olu, K., Riso, R., Sarradin, P.M., Segonzac, M., Vangriesheim, A. (2001). Variations in deep-sea
714 hydrothermal vent communities on the Mid-Atlantic Ridge near the Azores plateau. Deep-Sea Res. Part I
715 Oceanogr. Res. Pap. 48, 1325–1346.

717 Dufrene, M., Legendre, P. (1997). Species assemblages and indicator species: the need for a flexible asymmetrical
718 approach. Ecological monographs. 67(3):345-66.

720 Gebruk, A.V., Southward, E.C., Kennedy, H., Southward, A.J. (2000). Food sources, behaviour, and distribution
721 of hydrothermal vent shrimps at the Mid-Atlantic Ridge. J. Mar. Biol. Assoc. U.K. 80, 485–499.
722 http://dx.doi.org/10.1017/ S0025315400002186.

724 Hautala, S. Johnson, H.P., Pruis, M., Garcıá –Berdeal, I., Bjorklund, T. (2012). Low temperature
725 hydrothermal plumes in the near-bottom boundary layer at Endeavour Segment, Juan de Fuca Ridge.
726 Oceanography 25: 192–195.

728 Hessler, R.R., Smithey Jr, W.M., Keller, C.H. (1985). Spatial and temporal variation of giant clams, tubeworms
729 and mussels at deep-sea hydrothermal vents. Bull. Biol. Soc. Washington 6, 411–428.

731 Juniper, S.K., Matabos, M., Mihály, S., Ajayamohan, R.S., Gervais, F., Bui, A.O.V.(2013) A year in Barkley
732 Canyon: A time-series observatory study of mid-slope benthos and habitat dynamics using the NEPTUNE
733 Canada network. Deep Sea Res Pt II 92: 114–123.

735 Khripounoff, A., Comtet, T., Vangriesheim, A., Crassous, P. (2000). Near-bottom biological and mineral particle
736 flux in the Lucky Strike hydrothermal vent area (Mid-Atlantic Ridge). J. Mar. Syst. 25, 101–118,
737 http://dx.doi.org/10.1016/S0924- 7963(00)00004-X.

739 Khripounoff, A., Vangriesheim, A., Crassous, P., Segonzac, M., Lafon, V., Waren, A. (2008). Temporal variation
740 of currents, particulate flux and organism supply at two deep-sea hydrothermal fields of the Azores Triple Junction.
741 Deep Sea Res. Part I55, 532–551, http://dx.doi.org/10.1016/j.dsr.2008.01.001.

743 Laës-Huon, A., Sarradin, P.M., Tanguy, V., Cannat, M. (2015). CHEMINI total dissolved iron concentrations
744 from the EMSO-Azores observatory, 2011-2012. Sismer. http://doi.org/10.12770/14617ece-f7c6-4979-a171-
745 b497cfb8c413

747 Laes-Huon, A., Cathalot, C., Legrand, J., Tanguy, V., Sarradin, P.M. (2016). Long-Term In Situ Survey of
748 Reactive Iron Concentrations at the EMSO-Azores Observatory. IEEE Journal of Oceanic Engineering, (99), 1-
749 9.http://doi.org/10.1109/JOE.2016.2552779

751 Le Bris, N., Govenar, B.W., Legall, C. Fisher, C. (2006). Variability of physicochemical conditions in 9º50'N
752 EPR diffuse flow vent habitats. Mar Chem 98(2–4): 167–182.

754 Lee, R.W., Robert, K., Matabos, M., Bates, A.E., Juniper, S.K. (2015). Temporal and spatial variation in
755 temperature experienced by macrofauna at Main Endeavour hydrothermal vent field. Deep Sea Research Part I:
756 Oceanographic Research Papers. 31;106:154-66.

758 Legendre, P. (2012). Whittaker-Robinson periodogram. R program and documentation available on Web page
759 www.numericalecology.com.

761 Legendre, P., Legendre, L. (2012). Numerical ecology. Third English Edition. Elsevier Ed. p. 306

763 Luther, G., Gartman, A., Yücel, M., Madison, A., Moore, T., Nees, H., Nuzzio, D., Sen, A., Lutz, R., Shank, T.,
764 Fisher, C. (2012). Chemistry, temperature, and faunal distributions at diffuse-flow hydrothermal vents: comparison
765 of two geologically distinct ridge systems. Oceanography 25, 234–245. http://dx.doi.org/
766 10.5670/oceanog.2012.22.
767

768 Lutz, R.A., Shank, T.M., Luther III, G.W., Vetriani, C., Tolstoy, M., Nuzzio, D.B., Moore, T.S., Waldhauser, F.,
769 Crespo-Medina, M. Chatziefthimiou, A.D., Annis, E.R. (2008). Interrelationships between vent fluid chemistry,
770 temperature, seismic activity, and biological community structure at a mussel-dominated, deep-sea hydrothermal
771 vent along the East Pacific Rise. Journal of Shellfish Research. 27(1):177-90.

773 Martell, K.A., Tunnicliffe, V., Macdonald, I.R. (2002) Biological features of a buccinid whelk (Gastropoda,
774 Neogastropoda) at the Endeavour vent fields of juan de Fuca Ridge, Northeast Pacific. J Molluscan Stud 68:45–
775 53.

777 Matabos, M., Cuvelier, D., Brouard, J., Shillito, B., Ravaux, J., Zbinden, M., Barthelemy, D., Sarradin, P.M.,
778 Sarrazin, J. (2015). Behavioural study of two hydrothermal crustacean decapods: *Mirocaris fortunata* and
779 *Segonzacia mesatlantica*, from the Lucky Strike vent field (Mid Atlantic Ridge). Deep-sea Research part II
780 (doi:10.1016/j.dsr2.2015.04.008)

782 Matabos, M., Bui, A.O., Mihály, S., Aguzzi, J., Juniper, S.K., Ajayamohan, R.S. (2014). High-frequency study of
783 epibenthic megafaunal community dynamics in Barkley Canyon: A multi-disciplinary approach using the
784 NEPTUNE Canada network. Journal of Marine Systems. 28;130:56-68.

786 Mullineaux, L.S., Peterson, C.H., Micheli, F., Mills, S.W. (2003). Successional mechanism varies along a gradient
787 in hydrothermal fluid flux at deep-sea vents. Ecol. Monogr. 73, 523–542. http://dx.doi.org/10.1890/02-0674.

789 Naylor, E. (1985). Tidally rhythmic behaviour of marine animals. Symp. Soc. Exp. Biol., 39: 63-93.

791 Nees, H.S., Moore, T.S., Mullaugh, K.M., Holyoke, R.R., Janzen, C.P., Ma, S., Metzger, E., Waite, T.J., Yücel,
792 M., Lutz, R.A., Shank, T.M., Vetriani, C., Nuzzio, D.B., Luther, G.W.III (2008). Hydrothermal vent mussel habitat
793 chemistry, pre- and post-eruption at 9º5 North on the East Pacific Rise. J. Shellfish Res. 27: 169–175;
794 10.2983/0730-8000.

796 Puillat, I., Lanteri., N, Drogou, J.F., Blandin, J., Géli, L., Sarrazin, J., Sarradin, P.M., Auffret, Y., Rolin, J.F., Léon,
797 P. (2012). Open-Sea Observatories: A New Technology to Bring the Pulse of the Sea to Human Awareness. In:
798 Marcelli M editor. Oceanography, ISBN: 978-953-51-0301-1, InTech pp. 3-40

800 Sarradin, P.M., Legrand, J., Cannat, M .(2015). Temperature (°C) and dissolved oxygen concentrations data
801 from the EMSO-Azores observatory, 2011-2012. Sismer. http://doi.org/10.12770/6b8c0453-b03d-4ca2-8bdf-
802 084cf85ab0f1

804 Sarrazin, J., Blandin, J., Delauney, L., Dentrecolas, S., Dorval, P., Dupont, J., Legrand, J., Le Gall, C., Le Roux,
805 D., Hamon, M., Sudreau, J.P., Leon, P., Leveque, J.P., Rodier, P., Vuillemin, R., Sarradin, P.M. (2007) TEMPO:
806 A new ecological module for studying deep-sea community dynamics at hydrothermal vents. OCEANS '07
807 IEEE, Aberdeen, June 2007. Proceedings no. 061215-042.

809 Sarrazin, J., Cuvelier, D., Peton, L., Legendre, P., Sarradin, P.M. (2014). High-resolution dynamics of a deep-sea
810 hydrothermal mussel assemblage monitored by the EMSO-Açores MoMAR observatory. Deep-Sea Research I 90,
811 62–75

813 Sarrazin, J., Legendre, P., De Busserolles, F., Fabri, M.C., Guilini, K., Ivanenko, V.N., Morineaux, M., Vanreusel
814 ,A., Sarradin, P.M. (2015). Biodiversity patterns, environmental drivers and indicator species on a high-
815 temperature hydrothermal edifice, Mid-Atlantic Ridge. Deep Sea Research Part II: Topical Studies in
816 Oceanography. 121:177-92.

818 Shank, T.M., Fornari, D.J., Von Damm, K.L., Lilley, M.D., Haymon, R.M., Lutz, R.A. (1998). Temporal and
819 spatial patterns of biological community development at nascent deep-sea hydrothermal vents (9° 50N, East
820 Pacific Rise). Deep Sea Res Pt II 45: 465–515.

822 Thomsen, L., Barnes, C., Best, M., Chapman, R., Pirenne, B., Thomson, R., Vogt, J. (2012). Ocean circulation
823 promotes methane release from gas hydrate outcrops at the NEPTUNE Canada Barkley Canyon node. Geophys
824 Ress Lett 39: L16605
825

826 Tivey, M.K., Bradley, A.M., Joyce, T.M., Kadko, D. (2002). Insights into tide-related variability at seafloor
827 hydrothermal vents from time-series temperature measurements. Earth Planet Sci Lett 202:693–707
828

829 Tunnicliffe, V., Embley, R.W., Holden, J., Butterfield, D.A., Massoth, G., Juniper, S.K. (1997). Biological
830 colonization of new hydrothermal vents following an eruption on Juan de Fuca Ridge. Deep Sea Res Pt I 44(9-
831 10): 1627–1644.
832

833 Tunnicliffe, V., Garrett, .J, Johnson, H., (1990). Physical and biological factors affecting the behaviour and
834 mortality of hydrothermal vent tubeworms (vestimentiferans). Deep Sea Res 37(1): 103–125
835
836 Vuillemin, R., Le Roux, D., Dorval, P., Bucas, K., Sudreau, J.P., Hamon, M., Le Gall,C., Sarradin, P.M., (2009).
837 CHEMINI: A new in situ CHEmical MINIaturized analyzer. Deep Sea Res Pt I 56(8): 1391–1399
838

839 Zambrano-Bigiarini, M. (2012). hydroTSM: Time series management, analysis and interpolation for
840 hydrological modelling. R package version 0.3–6. Available: http://CRAN.R-project.org/package=hydroTSM.
841
842
843
844
845
846
847
848
849
850
851
852
853
854
855
856
857
858
859
860
861
862
863
864
865
866
867
868
869
870
871
872
873
874
875
876
877
878
879
880
881
882
883
884

Figures

885
886

887
888 **Fig 1. Location of the two study-sites along with some other well-known vent fields for reference purposes. TEMPO is**
889 **located at the Lucky Strike vent field on the MAR, whilst TEMPO-mini is at Main Endeavour Field on the Juan de**
890 **Fuca Ridge (NEP). For more details of the exact location of the observatories within the hydrothermal vent fields see**
891 **Matabos et al (2015) for MAR and Cuvelier et al. (2014) for NEP.**
892
893
894
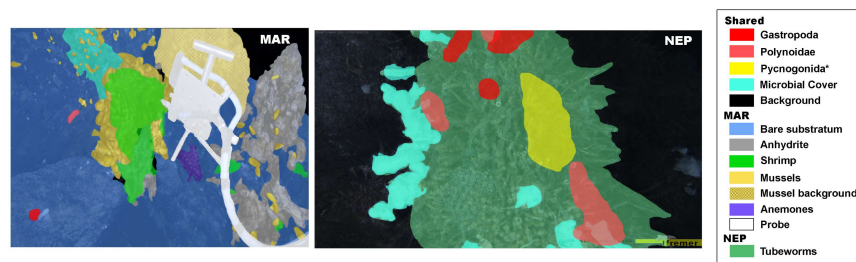
895
896 **Fig 2. Sketch of the fields of view (FOV) as recorded by the ecological observatory modules for MAR and NEP with all**
897 **features assessed. Taxa or other features that are shared between the two have the same colour codes. Gastropoda**
898 **applies to Buccinidae for NEP and bucciniform Turridae on MAR. '*' is a shared taxon but not visible on MAR due to**
899 **the scarce presence and low densities. 'Mussel background', 'background' and 'probe' were not included in the surface**
900 **calculations. The white arrow represents the fluid flow exit and direction. No visible emission was observed on NEP.**
901 **Visiting fish and crab species were not included (Table 2). Crab presence on MAR tends to correspond predominantly**
902 **to shrimp distribution (Matabos et al., 2015).**
903
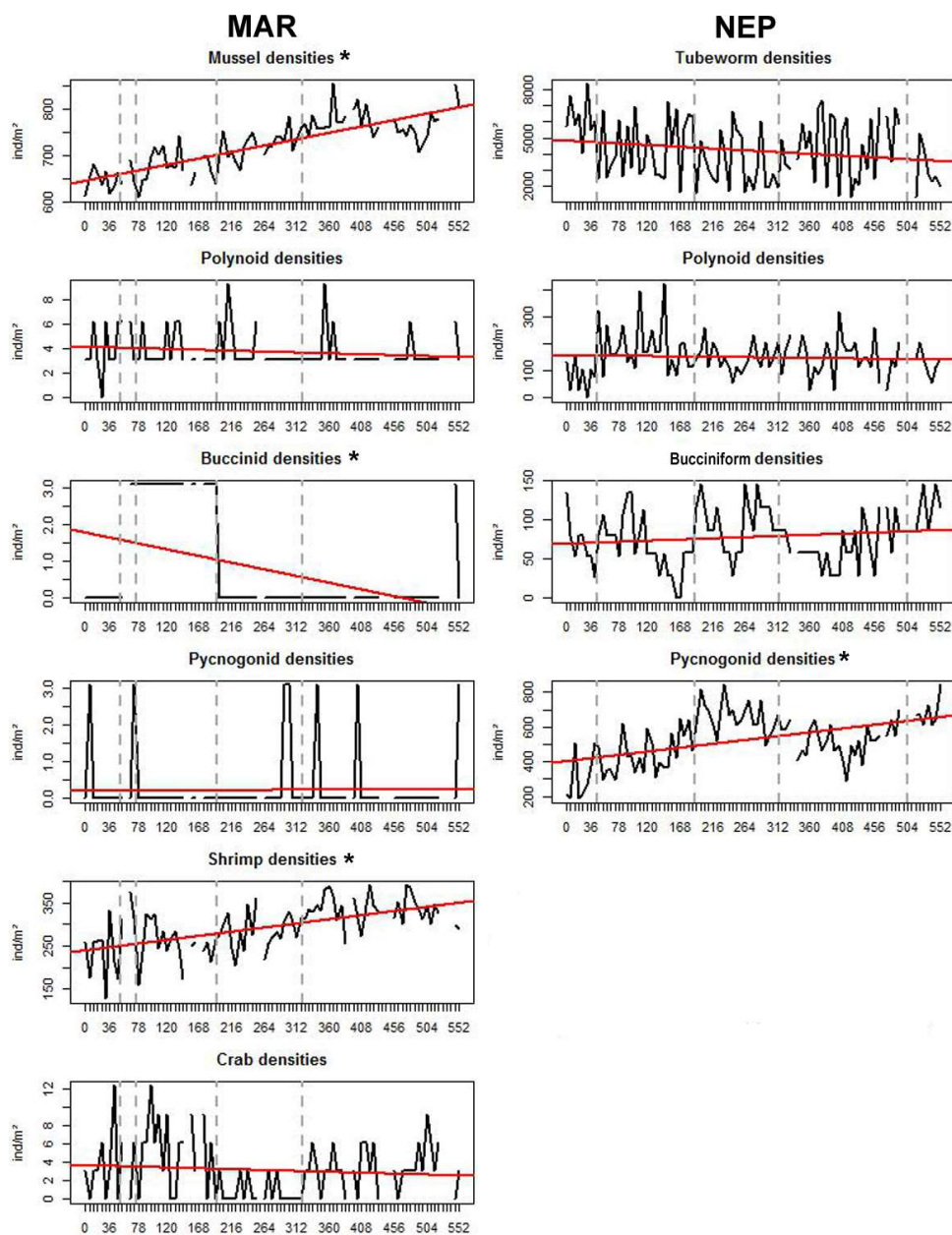
Fig. 3. Temporal variations in faunal densities for MAR and NEP along with trend lines (in red) and MRT temporal groups (grey vertical dotted bars), x-axis are hours, sampling frequency every 6h. Taxa with significant trends are marked with a *.
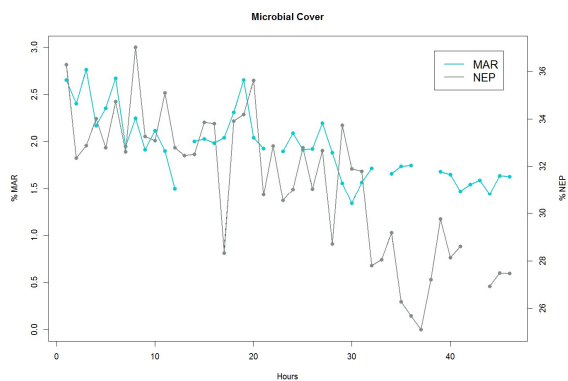
Fig. 4. % Microbial cover every 12h, for the imagery period analysed, X-axis contains periods, 1 period=12h
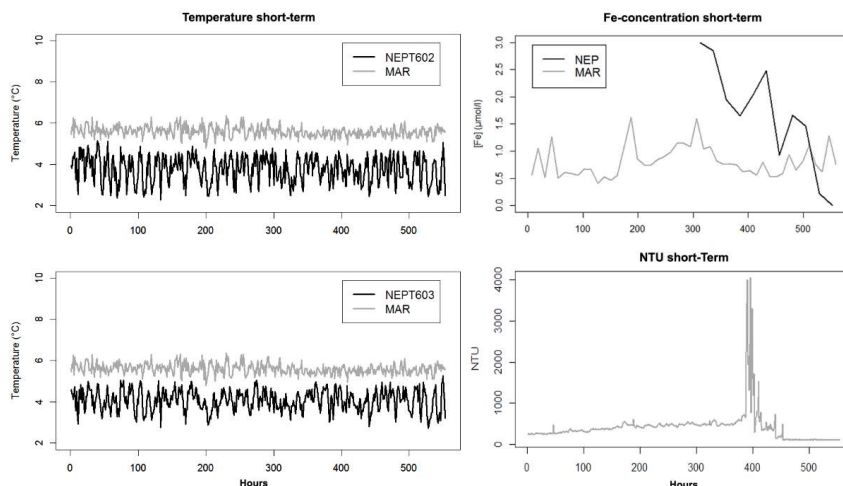
Fig. 5. Environmental variables averaged per hour during imagery analysis period. Variables measured at both deployment sites are presented in the same graphic (temperature and Fe). Fe has a daily frequency for the MAR but a 12h frequency for the NEP and recording times differ. NTU was only available for the MAR.
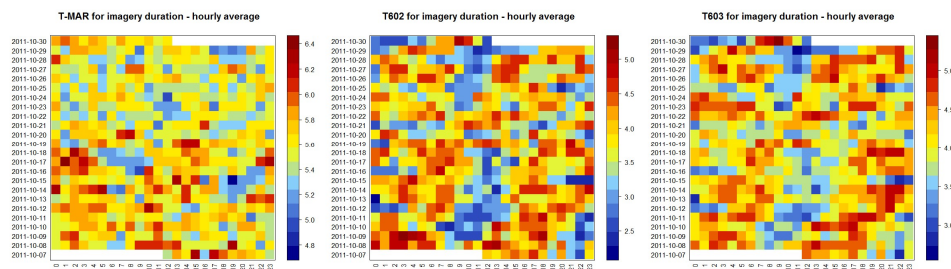
Fig. 6. Hourly temperature values for T602 and T603 probes from NEP and the MAR temperature probe. Red are higher temperatures while blue are lowest temperatures. Dates correspond to the duration of the imagery analyses (23 days).
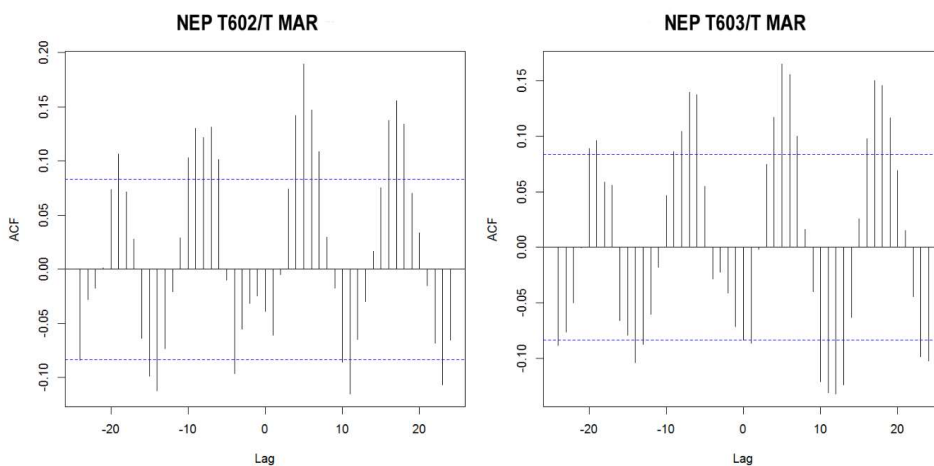
930
931 Fig. 7. Cross correlations of the hourly temperature values. ACF=autocorrelation function on Y-axis, 1 lag equals 1
932 hour on X-axis. Comparisons are made between the MAR probe and T602 on left side and MAR and T603 on the
933 right.
934
935

955 Fig. 8. RDA ordinations featuring Hellinger transformed faunal densities and standardised environmental variables
956 both at a 6h frequency. Temporal splits groups were colour-coded in the ordination plots.
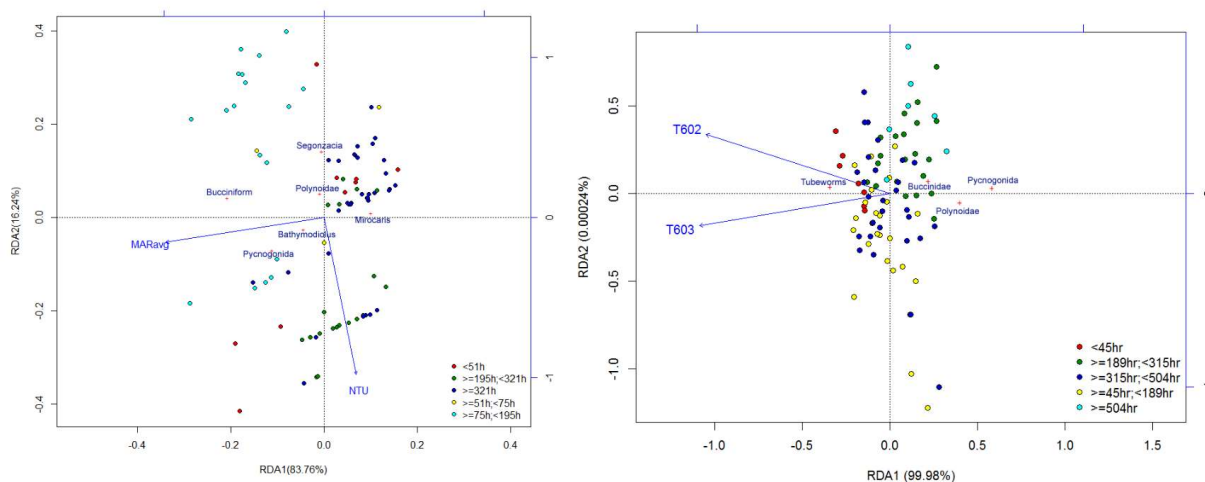
957
958
959
960
961
962
963
964
965
966
967
968
969
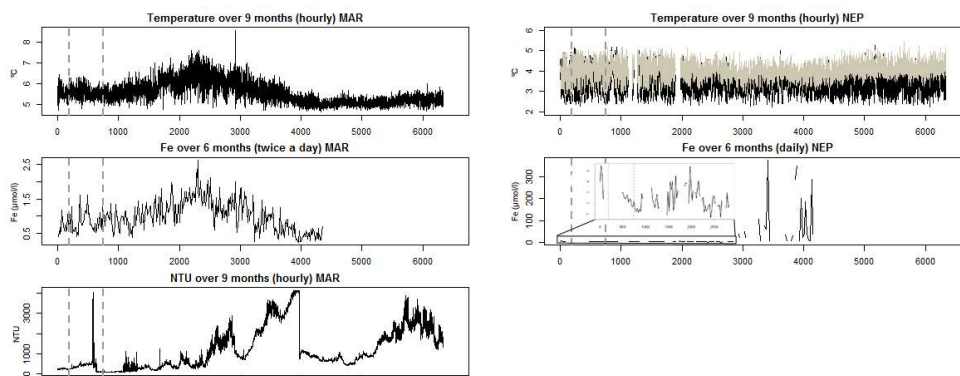
970
971 **Fig. 9. Long-term environmental variable overview, spanning 9 months. Dotted vertical lines delineate the period for**
972 **which the images have been analysed.**
973
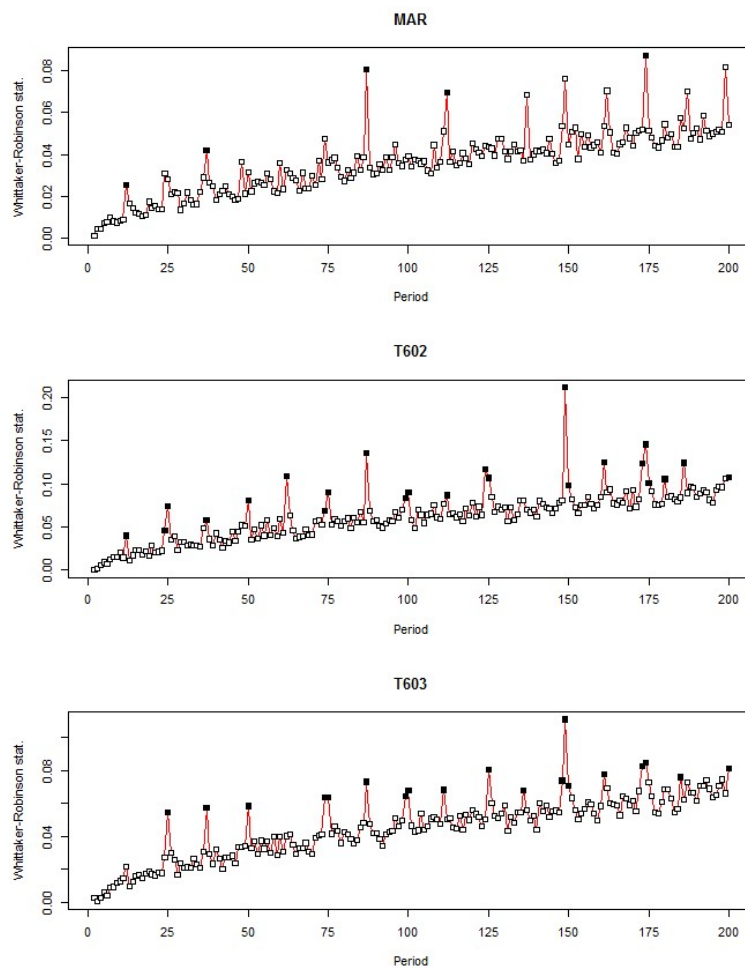
974
975 **Fig. 10. Periodogram analyses of ~9 months of hourly temperature measurements for MAR and NEP (T602 and T603)**
976 **represented as a one-week period (equalling 200h). Black squares indicate periods significant at the 5% level.**

977
978

Appendix/Supplementary figures
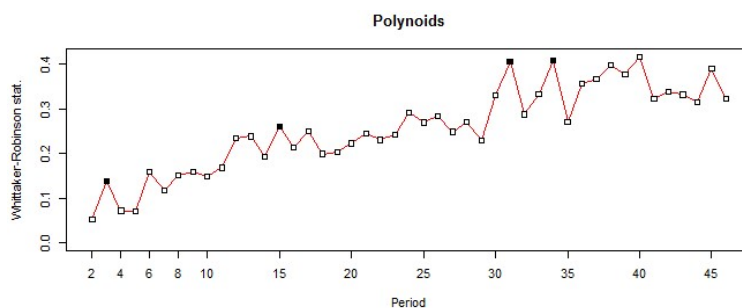
979
980 **Fig. S1. MAR faunal periodogram on polynoid densities with a 6h frequency (1 period on x-axis=6h), all other taxa**
981 **had no significant periodicities and were thus not shown**
982
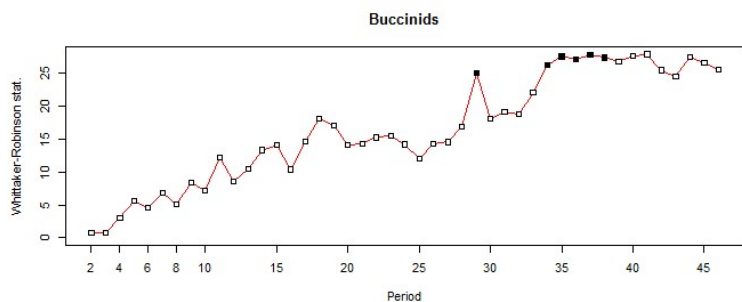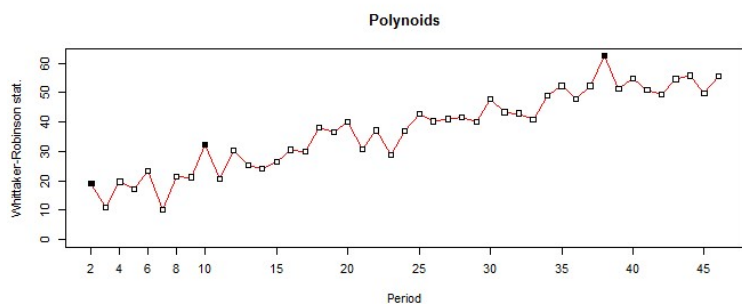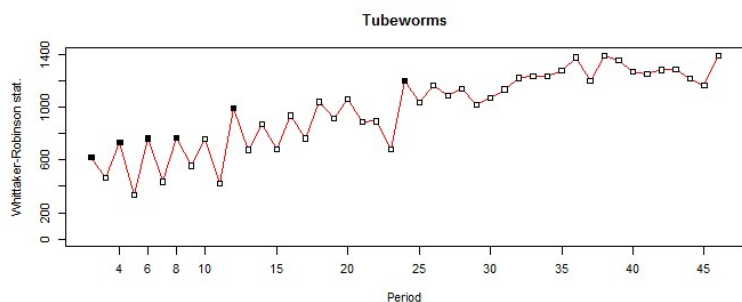
983
984 **Fig. S2. NEP Faunal periodograms featuring significant periodicities. Taxa presented are tubeworm, polynoid and**
985 **buccinid densities with a 6h frequency for the MAR (1 period on x-axis=6h), pycnogonids showed no significant**
986 **periodicities and were not shown.**
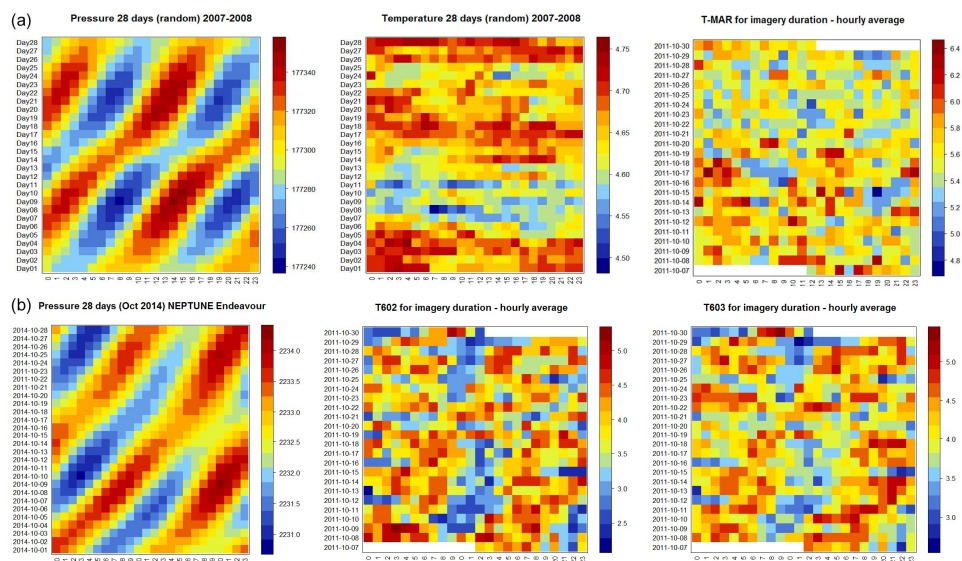
Fig S3. Comparison of cyclicity in pressure data and temperature for MAR (a) and NEP (b) Red are higher values
while blue are lowest values. Pressure data for MAR originates from 2007-2008 and was recorded at Seamon West of
the EMSO-Azores observatory and represents a random 28 day (lunar) period (data courtesy of Valerie Ballu) .
Pressure data for NEP were downloaded from ONC Portal from the BPR (NRCan Bottom Pressure Recorder
deployed at MEF/Endeavour) ("Ocean Networks Canada Data Archive http://www.oceannetworks.ca, Total Pressure
data from 1-29 Oct 2014, University of Victoria, Canada, Downloaded on 16 Jun 2015"). A random selection of 28
days in October 2014 is presented here (no earlier data were available).

Tables

Table 1: Overview of the location, data recorded and the recording resolutions of all variables of the two observatories on the NEP and MAR. *limited usefulness due to issues related to correctly calculate the oxygen concentrations.

	TEMPO MoMAR (MAR) Wireless	TEMPO-mini NEPTUNE (NEP) Cabled
	2011-2012	2011-2012
Coordinates Lat Coordinates Long	N 37° 17.3321' W 32° 16.5334'	N 47°56.9574' W 129°05.8998'
Depth	1694 m	2168 m
Imagery	4 min. every 6 hrs (0h, 6h, 12h, 18h UTC)	Continuous for ~23 days followed by 30 min every 4hrs (2h, 6h, 10h, 14h, 18h , 22h UTC)
Temperature	1 measurement every 5 min	1 measurement every 30 seconds
Optode (Oxygen + temperature) *	1 measurement every 15 min	1 measurement every 15 min
Chemini Fe	twice a day	twice a day/daily
Turbidity	1 measurement every 15 min	/

1042 **Table 2: Overview of the characteristics of the images analysed such as surface covered and taxa assessed. * are visiting**
1043 **predators. The observation surface on the MAR is about 10 times larger than that on the NEP.**

	TEMPO MoMAR (MAR) **2011-2012**	**TEMPO-mini NEPTUNE (NEP)** **2011-2012**
# Images (6hr frequency)	84 (93-9 gaps)	88 (93-5 gaps)
Surface filmed	~0.3802 m² (ca. 52.8 x 72 cm)	~0.0661 m²
Surface analysed (see fig. X)	~0.322 m²	~0.0355 m² (ca. 20 x 18 cm)
Taxon densities		
Engineering species	Mollusca - Mytilidae (Mussels) *Bathymodiolus azoricus*	Polychaeta - Siboglinidae (Tubeworms) *Ridgeia piscesae*
Polychaeta	Polynoidae Multiple species (Desbruyères et al. 2006)	Polynoidae Multiple species (Cuvelier et al. 2014)
Arthropoda	*Mirocaris fortunata* *Segonzacia mesatlantica* (crabs) Ammotheidae	/ *Macroregonia macrochira* (spider crab)* Ammotheidae
Gastropoda	Turridae *Phymorynchus* sp. (bucciniform)	Buccinidae *Buccinum thermophilum*
Pisces	*Cataetyx laticeps**	*Pachycara* sp.*
Surface coverage	% Microbial mats (12 h frequency)	% Microbial mats (12 h frequency)

1044

1045

1046

1047

1048

1049   **Table 3. Temporal split groups for MAR and NEP based on MRT analysis.**

MAR		NEP		Timespan
<51h	n=9	< 45 h	n=8	~ 2 days
≥ 51 h, <75 h	n=3	≥ 45, < 189 h	n=24	> 2 days, < 8 days
≥ 75h, < 195 h	n=18			(spanning ca. 6 days)
≥ 195 h, < 321h	n=20	≥ 189 h, < 315 h	n=21	>8 days, < ~ 13 days (spanning ca. 5 days)
≥ 321 h - 553	n=34	≥ 315 h, < 504 h	n=28	> ~13 days, <21 days for NEP (spanning ~8 days) > ~13 days, 23 days (10 days for MAR)
		≥ 504 h - 553	n=7	> 21 days till end of recordings (~2days)

1050

1051

1052   **Table 4. Mean, maximum and minimum temperatures as measured by the probes and, for comparison purposes**
1053   **rescaled to ambient seawater temperature (highlighted in grey). Variance and standard-deviations are presented as**
1054   **well. Bold values represent highest values which tend to change if rescaled to ambient seawater temperature or not.**

	Mean		Max		Min		Var	stdev
MAR	**5.59 °C**	1.59°C	**6.36 °C**	2.36°C	**4.79 °C**	**0.79°C**	0.066	0.258
NEPT602	3.76°C	1.76°C	5.14 °C	3.14°C	2.28 °C	0.28°C	0.259	**0.645**
NEPT603	4.07 °C	**2.07°C**	5.27 °C	**3.27°C**	2.73 °C	0.73°C	**0.416**	0.509

1055

1056

1057